PAPER • OPEN ACCESS

Stability analysis of plasma waves driven by runaway electrons in tokamak hot plasmas

To cite this article: C. Castaldo *et al* 2024 *Nucl. Fusion* **64** 086003

OPEN ACCESS
IOP Publishing | International Atomic Energy Agency
Nuclear Fusion
Nucl. Fusion **64** (2024) 086003 (13pp)
https://doi.org/10.1088/1741-4326/ad4ef6

Stability analysis of plasma waves driven by runaway electrons in tokamak hot plasmas

C. Castaldo[1,*], L. Della Volpe[2], R. Fedele[2], W. Bin[3], P. Buratti[1,4], A. Cardinali[4,5], F. Napoli[1], M. Marinucci[1,6], G. Apruzzese[1], C. Cianfarani[1], E. Giovannozzi[1] and O. Tudisco[1]

[1] ENEA, Fusion and Nuclear Safety Department, Frascati (Rome), Italy
[2] Dipartimento di Fisica and INFN, Università Federico II, Napoli, Italy
[3] ISTP-CNR, Institute for Plasma Science and Technology, National Research Council (ISTP-CNR), Milan, Italy
[4] INAF-IAPS, Roma, Italy
[5] CNR, Istituto Sistemi Complessi, Politecnico di Torino, Torino, Italy

E-mail: carmine.castaldo@enea.it

Received 6 February 2024, revised 26 April 2024
Accepted for publication 22 May 2024
Published 18 June 2024

Abstract

The local stability analysis of plasma waves driven by runaway electrons (REs) has been performed considering hot plasma Maxwellian background, with electron and ion temperatures of the order of 1 keV. It is shown that hot plasma waves, namely electron plasma waves (EPWs) and ion Bernstein waves (IBWs) can be driven unstable by RE at their coalescence frequency via Cherenkov resonance by RE with energy distribution peaked at about 8 MeV. A skew-normal distribution is used as a model of the RE energy distribution. The EPW and IBW couples of waves occur between any successive ion-cyclotron harmonics frequencies nf_{ci}, above the lower hybrid resonance. At their confluence, the perpendicular group velocity vanishes and significant RF emissions are expected. The frequency gap between two successive confluences is $\sim f_{ci}$. Groups of RF line emissions, separated by almost constant frequency gap $\sim f_{ci}/2$ are detected during various quiescent runaway plasma discharges in the FTU tokamak. The analysis of a specific discharge suggests that the frequencies of the line emissions observed and the frequencies occurring at the EPW-IBW confluences are in reasonable agreement. A possible explanation of the line emissions with $\sim f_{ci}/2$ gap in terms of nonlinear mode coupling is proposed.

Keywords: runaway, waves, tokamak, instabilities

(Some figures may appear in colour only in the online journal)

[6] Retired.
[*] Author to whom any correspondence should be addressed.

1. Introduction

The production of runaway electrons (REs) in fusion reactors based on the tokamak concept is a potential risk factor, since the RE might damage the plasma facing components. In ITER, during plasma disruptions, 12 MA RE beams can be formed [1], with kinetic energy of the electrons of several MeV [2]. To minimize the RE effects occurring upon disruptions, mitigation techniques are extensively pursued in current tokamaks, accompanied by the development of suitable RE diagnostics, as discussed in the review paper [3] concerning the physics of RE in tokamaks. In recent years, the detection of radiofrequency (RF) waves emitted in the presence of RE in tokamaks opened the search for a new kind of diagnostics. The identification of RF waves driven by RE is indeed a promising method to infer the characteristics of the RE distribution and a tool to detect RE in the early phase of a plasma discharge. In addition, a new method of RE mitigation by injection of RF waves is envisaged, to stimulate the emission of plasma waves at the expenses of the RE energy. Whistler waves (WWs) driven by RE were observed for the first time in the DIII-D tokamak [4, 5]. The fast dynamics of RF emissions in FTU plasmas with RE has been investigated in [6]. RE driven instabilities identified as lower hybrid waves (LHWs) were observed for the first time in FTU under ITER-relevant conditions [7]. Details of the relevant detection system are reported in [8]. RF emissions during plasma discharges with RE have been observed in COMPASS [9–11] and KSTAR [12]. More recent studies on this field are proposed in [13–15]. The stability analysis of plasma waves driven by RE, within the cold plasma approximation, was performed in [16] and complemented by the ray-tracing technique to evaluate the amplification of the waves, statistically appreciated from a set of initial wave parameters. The wave interactions with RE, driving the instabilities, occur at the resonances

$$\omega - k_{\parallel} v \mu - n\frac{\omega_{ce}}{\gamma} = 0. \tag{1}$$

Here ω and $k_{\parallel}$ are, respectively the angular frequency and the wavenumber parallel to the equilibrium magnetic field $\boldsymbol{B}$, $v = |\mathbf{v}|$ is the absolute value of the velocity $\mathbf{v}$ of the RE, $\mu = \cos\theta$, θ is the pitch angle, i.e. the angle between $\boldsymbol{B}$ and $\mathbf{v}$, n is an integer number, $\omega_{ce} = -e|\boldsymbol{B}|/(m_e c)$ is the electron cyclotron angular frequency, $e > 0$ is the elementary charge, m_e is the mass of the electrons, c is the velocity of the light in vacuum, and $\gamma = \left[1 - v^2/c^2\right]^{-1/2}$ is the relativistic parameter. We adopt cgs units. The main channels driving the instabilities are the Cherenkov resonance ($n = 0$) and the anomalous Doppler resonance ($n = 1$) [17, 18]. The free energy source of the instabilities is due to the anisotropy or to the presence of a local maximum of the RE distribution function in the momentum space. The latter can be produced as a result of the RE acceleration due to the static toroidal electric field parallel in the presence of the diffusion and drag associated to the collisions and the emission of the synchrotron radiation, as discussed in [3] and in the references quoted therein. Based on a quasilinear model, the presence of an attractor in the momentum space was predicted in [19] by a self-consistent analysis of the excitation of kinetic instabilities and the scattering of resonant electrons, explaining the excitation of WW in the quiescent RE experiments at DIII-D [4, 5]. The occurrence of non-monotonic energy distributions during the current ramp up in the FTU tokamak was predicted in [20], suggesting a time evolution towards quasi-monochromatic distributions. In [7], assuming a peak in the energy distribution of RE, modeled by a Gaussian shape, allowed to evaluate the growth rates of LH waves driven unstable via the Cherenkov resonance. In the present work, we perform the local linear stability analysis of plasma waves excited by RE, in Maxwellian hot plasma background. This allows investigating the stability of plasma waves that cannot be described within the cold plasma approximation, e.g. electron plasma waves (EPWs) and ion Bernstein waves (IBWs). The numerical code REDHPW (Runaway Electron Driven Hot Plasma Waves) has been developed to perform the stability analysis. It is described in section 2. We introduce a new kind of RE distribution function, based on a skew normal energy distribution, which seems appropriate in the presence of a peak in the momentum space. A benchmark of REDHPW in the limit of low plasma temperature with a scenario discussed in [16] within the cold plasma approximation is also proposed. In section 3, we perform the linear stability analysis for plasma scenarios typical of FTU in the presence of RE, utilizing the REDHPW code and the skew normal distribution above mentioned. We show, for the first time, that EPW and IBW hot plasma waves can be driven unstable by RE. In section 4, we report experimental results concerning the detection of RF emissions during FTU discharges with RE, which might confirm the excitation of hot plasma waves by RE. Line emissions separated by an almost constant frequency gap, which correspond to the ion cyclotron frequency or its half, are observed in various discharges, both during the current ramp and in the flat top. We analyze in some detail one of them, comparing the spectrogram of the RF emissions detected with the theoretical predictions. Section 5 is devoted to the summary and the discussion of the results.

2. Stability analysis by REDHPW code

The REDHPW code implements approximate solutions of the electromagnetic linear wave equation for homogeneous Maxwellian magnetized non-relativistic plasma background, with multiple ion species of charge q_i and mass m_i, in the presence of a given distribution function of RE. The wave electromagnetic field is assumed quasi-monochromatic and approximated by the real part of the complex electric and magnetic fields, respectively $\boldsymbol{E}e^{i(\boldsymbol{k}\cdot\boldsymbol{r}-\omega t)}$ and $\boldsymbol{B}e^{i(\boldsymbol{k}\cdot\boldsymbol{r}-\omega t)}$. It is assumed, without any lack of generality, that the real part of the angular frequency ω is positive. The linear wave equation is

$$\overline{\overline{\Lambda}} \cdot \boldsymbol{E} = \mathbf{0} \tag{2}$$

Here the Cartesian components of the tensor $\overline{\overline{\Lambda}}$ are given by

$$\Lambda_{\alpha\beta} = k_\alpha k_\beta c^2 - k^2 c^2 \delta_{\alpha\beta} + \omega^2 \overline{\overline{\varepsilon}}_{\alpha\beta} \tag{3}$$

$\overline{\overline{\varepsilon}} = \overline{\overline{\varepsilon}}_{\mathrm{M}} + \overline{\overline{\chi}}_{\mathrm{RE}}$, where $\overline{\overline{\varepsilon}}_{\mathrm{M}} = I + \overline{\overline{\chi}}_e + \sum_i \overline{\overline{\chi}}_i$, is the dielectric tensor, which includes the susceptibilities of the Maxwellian plasma electrons, respectively $\overline{\overline{\chi}}_e$ and $\overline{\overline{\chi}}_i$, as well the susceptibility $\overline{\overline{\chi}}_{\mathrm{RE}}$ of the RE . We adopt the Stix reference frame, with Cartesian axis X aligned along the component of the wavenumber $\boldsymbol{k}$ perpendicular to the static magnetic field $\boldsymbol{B}_o$ and the axis Z parallel to $\boldsymbol{B}_o$. The Cartesian components of the susceptibilities $\overline{\overline{\chi}}_e$ and $\overline{\overline{\chi}}_i$ for collisionless Maxwellian plasma, are expressed by analytic formulas in standard textbooks, e.g [21], given the wave angular frequency and wavenumber, the absolute magnetic field $|\boldsymbol{B}_o|$, the temperature $s\,T_{e,i}$ and the density $n_{e,i}$ of the electrons (subscript e) and the ions (subscript i), with electric charge $q_{e,i}$ and mass $m_{e,i}$. The RE susceptibility $\overline{\overline{\chi}}_{\mathrm{RE}}$ components are calculated numerically by integrals in the momentum space based on the general expression of the susceptibility tensor for relativistic particles [21]. If both the orderings $|\omega_i| \ll \omega_r$ and $|\overline{\overline{\varepsilon}}^{A}_{\alpha\beta}| \ll |\overline{\overline{\varepsilon}}^{H}_{\alpha\beta}| \forall \alpha,\ \beta$ are fulfilled, a Taylor expansion provides approximate solutions of the wave equation [22] (here the subscripts i and r denote, respectively, the imaginary and the real components and the superscripts A and H indicate, respectively, the anti-Hermitian and the Hermitian part). For any given parallel refractive index $N_\parallel = N_z = k_z c/\omega_r$ and for any value of ω_r, normal plasma modes branches are identified by REDHPW, calculating the perpendicular refractive index $N_\perp = N_x = k_x c/\omega_r$ as numerical solutions of the wave dispersion equation

$$\det \overline{\overline{\Lambda}}^{H} = 0 \tag{4}$$

$$\text{where } \Lambda^{H}_{\alpha\beta} = N_\alpha N_\beta - N^2 \delta_{\alpha\beta} + \overline{\overline{\varepsilon}}^{H}_{\alpha\beta}. \tag{5}$$

We neglect the contribution of the RE to the Hermitian dielectric tensor, assuming that the RE density n_b is orders of magnitude smaller than the plasma density n_e. In the FTU quiescent discharges with RE, typical values are of the order of 0.1 % n_e. The Hermitian part of the dielectric tensor is calculated utilizing the analytic expression of the dielectric tensor $\overline{\overline{\varepsilon}}_{\mathrm{M}}$ for Maxwellian plasmas and the definition $\overline{\overline{\varepsilon}}^{\mathrm{H}} = (\overline{\overline{\varepsilon}}_{\mathrm{M}} + \overline{\overline{\varepsilon}}^{+}_{\mathrm{M}})/2$. Here $\overline{\overline{\varepsilon}}^{+}_{M}$ indicates the adjoint tensor of $\overline{\overline{\varepsilon}}_{\mathrm{M}}$, i.e. the transpose of the complex conjugate of the matrix defining $\overline{\overline{\varepsilon}}_{\mathrm{M}}$. For each normal plasma mode, the electric field polarization is obtained solving the wave equation

$$\overline{\overline{\Lambda}}^{\mathrm{H}} \cdot \boldsymbol{E} = \boldsymbol{0}. \tag{6}$$

The magnetic field $\boldsymbol{B}$ can be then obtained from $\boldsymbol{E}$ by the Faraday law. The imaginary part of the angular frequency, based on the anti-Hermitian part $\overline{\overline{\varepsilon}}^{\mathrm{A}}$ of the dielectric tensor, is given by

$$\omega_i = i \frac{E^*_\alpha E_\beta \omega^2 \varepsilon^{\mathrm{A}}_{\alpha\beta}}{E^*_\alpha E_\beta \frac{\partial}{\partial\omega} \omega^2 \varepsilon^{\mathrm{H}}_{\alpha\beta}}. \tag{7}$$

The normal plasma waves are unstable growing modes if $\omega_i > 0$ or stable damped modes if $\omega_i < 0$. The anti-Hermitian part of the Maxwellian dielectric tensor, namely $\overline{\overline{\varepsilon}}^{\mathrm{A}}_{\mathrm{M}} = \overline{\overline{\varepsilon}}_{\mathrm{M}} - \overline{\overline{\varepsilon}}^{+}_{\mathrm{M}}/2$, includes the contribution due to the resonances of the Maxwellian electrons (subscript e) and ions (subscript i), namely

$$\omega_r - k_\parallel \mathrm{v}_{\parallel e,i} - n\Omega_{e,i} = 0. \tag{8}$$

Here $\Omega_{e,i} = (q_{e,i} B_o)/(m_{e,i} c)$ is the angular cyclotron frequency of the electrons and ions. In addition, $\varepsilon^{\mathrm{A}}_{\alpha\beta}$ includes the effects of the resonances of the relativistic RE, as given by equation (1).

These resonances correspond to poles in the integrals in the momentum space that determine the RE anti-Hermitian susceptibility $\overline{\overline{\chi}}^{\mathrm{A}}_{\mathrm{RE}}$ and are calculated numerically in the REDHPW code, following the Landau prescription. For computational purpose, it is convenient to express the components of $\overline{\overline{\chi}}^{\mathrm{A}}_{\mathrm{RE}}$ as integrals in the $(u,\ \mu)$ space (the RE distribution functions are assumed as independent on the gyro-angle). Here we define $u = p/(m_e c)$ as the normalized momentum of the RE. Owing to the Dirac delta distribution resulting from the Landau prescription to treat the resonance poles, the integrals over μ are calculated analytically, and only 1D numerical integrals over u are performed (an identical result is obtained by first performing the integrals over u analytically and then numerically the 1D integrals over μ). To include the effects of the collisions we adopt a quite simple approximation, i.e. the substitution $\omega \Rightarrow \omega + i\nu_e$ in the conductivity tensor of the electrons [16], where ν_e is the electron–ion collisional frequency given by

$$\nu_e = \frac{4\sqrt{2\pi}\,\Lambda_c e^4 n_e Z_{\mathrm{eff}}}{3 m_e^{1/2} T_e^{3/2}}. \tag{9}$$

Here Λ_c is a Coulomb logarithm, $Z_{\mathrm{eff}} = \sum_i Z_i^2 n_i/n_e$ is the effective charge, $Z_i = q_i/e$ is the ion charge number and T_e is in erg units. We adopt a simple evaluation of Λ_c, given by [23] with $\tilde{T}_e$ is measured in eV

$$\Lambda_c = 24 - \ln\left(n_e^{1/2} \tilde{T}_e^{-1}\right). \tag{10}$$

The Maxwellian dielectric tensor, including the effects of the collisions, is thus

$$\overline{\overline{\varepsilon}}^{\mathrm{M}}(\omega, \boldsymbol{k}) = I + \sum_i \overline{\overline{\chi}}_i(\omega, \boldsymbol{k}) + \frac{\omega + i\nu_e}{\omega} \overline{\overline{\chi}}_e(\omega + i\nu_e, \boldsymbol{k}). \tag{11}$$

Based on a Taylor expansion, as done to obtain ω_i in equation (7), the (positive) collisional damping rates are calculated in REDHPW utilizing the following expression

$$\Gamma_c = \left[-i \frac{E^*_\alpha E_\beta \omega^2 \chi^{A}_{\mathrm{ec},\alpha\beta}}{E^*_\alpha E_\beta \frac{\partial}{\partial\omega} \omega^2 \varepsilon^{H}_{\alpha\beta}} \right]_{\omega=\omega_r}. \tag{12}$$

Here the anti-Hermitian part of the electron susceptibility tensor due to the collisions is given by

$$\overline{\overline{\chi}}^{\mathrm{A}}_{\mathrm{ec}} = i\frac{\nu_e}{\omega_r}\left[\overline{\overline{\chi}}^{\mathrm{H}}_e(\omega_r,\boldsymbol{k}) + \omega_r\frac{\partial\overline{\overline{\chi}}^{\mathrm{H}}_e(\omega_r,\boldsymbol{k})}{\partial\omega_r}\right] \tag{13}$$

where $\overline{\overline{\chi}}^{\mathrm{H}}_e$ is the Hermitian part of the susceptibility tensor of the Maxwellian electrons.

As a final property of the normal plasma waves, their group velocities perpendicular ($v_{g\perp}$) and parallel ($v_{g\parallel}$) to the static magnetic field are calculated by the following expression [22]

$$\mathrm{v}_{g\perp} = -\frac{E^*_\alpha E_\beta\frac{\partial\Lambda^H_{\alpha\beta}}{\partial k_\perp}}{E^*_\alpha E_\beta\frac{\partial\Lambda^H_{\alpha\beta}}{\partial\omega_r}},\ \mathrm{v}_{g\parallel} = -\frac{E^*_\alpha E_\beta\frac{\partial\Lambda^H_{\alpha\beta}}{\partial k_\parallel}}{E^*_\alpha E_\beta\frac{\partial\Lambda^H_{\alpha\beta}}{\partial\omega_r}}. \tag{14}$$

The workflow of REDHPW is now summarized. The code requires in input the following data (1) the parameters of the Maxwellian distribution, namely n_e, n_i, q_i, m_i, T_e, T_i, B_o (2) the RE distribution function chosen among the three expressions indicated below and the relevant parameters (3) a regular mesh of values of $N_\parallel$ and ω_r to analyze the corresponding normal modes (4) the interval of values of $N_\perp$ where normal plasma modes are to be identified (5) a set of resonance numbers for the RE interactions with plasma waves. A double loop on $N_\parallel$ and ω_r is performed. As a first calculation, REDHPW identifies the values of $N_\perp$ corresponding to normal plasma modes by numerical solution of the wave dispersion equation (4), based on the implementation of the analytic expression of $\overline{\overline{\varepsilon}}^{\mathrm{H}}$. The electric field polarization for each normal plasma mode is then calculated by solving equation (6). For each normal plasma mode, the imaginary part of the angular frequency is then calculated by equation (7) and the collisional damping by equation (12). Finally, for each normal plasma mode, the group velocity is calculated, based on equation (14).

Though arbitrary RE distribution functions can be implemented in REDHPW, three kind of RE distribution function are now embedded in the code. The typical distribution for the RE avalanche regime with fixed spread of the pitch angle ($\sigma = const$):

$$f(u,\mu) = n_b\frac{e^{-u/u_o}}{u_o u^2}\frac{\sigma e^{-\sigma(1-\mu)}}{1-e^{-2\sigma}}. \tag{15}$$

Here n_b is the RE number density. A distribution function of the form (15) but with momentum-dependent spread of the pitch angle, obtained assuming $\sigma = \sigma_o u^2/\gamma$ where $\gamma = \sqrt{1+u^2}$ is the relativistic parameter.

A distribution proportional to a skew-normal distribution [24] vs. the energy, given by

$$f(E,\mu) = \frac{n_b}{C(E_p/\sigma_E,\alpha)}\frac{1}{\sigma_E}\varphi\left(\frac{E-E_p}{\sigma_E}\right)\Phi \times\left(\alpha\frac{E-E_p}{\sigma_E}\right)\frac{\sigma_\theta}{2\sinh\sigma_\theta}\exp(\sigma_\theta\mu). \tag{16}$$

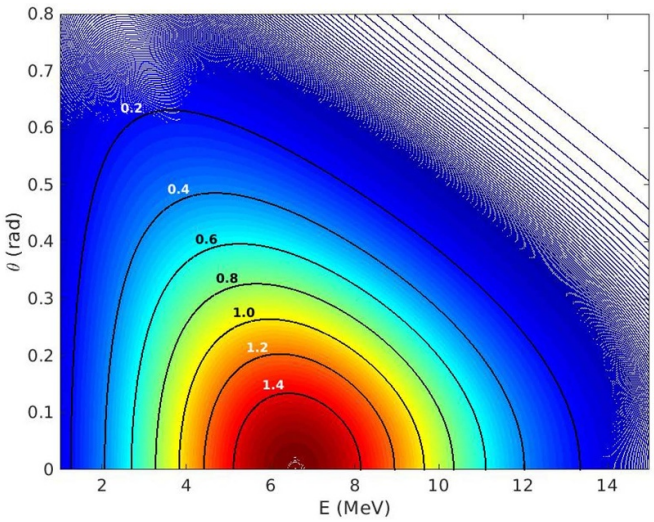

Figure 1. Contour plot of the function $f(E,\cos(\theta))/n_b$, with f given by equation (14). Here we consider the parameters $\alpha = 1.0$, $E_p = 3$ MeV, $\sigma_E = 4$ MeV, $\sigma_o = 1$.

Here $E = (\gamma-1)m_e c^2$ is the kinetic energy of the electrons, φ is the normal distribution, defined by $\varphi(x) = (2\pi)^{-1/2}\exp(-x^2/2)$, Φ is the relevant cumulative distribution, i.e. $\Phi(x) = [1+\mathrm{erf}(x/\sqrt{2})]/2$, where erf is the error function and $\sigma_\theta = \sigma_o u^2/\gamma$.

The normalization constant C is defined as

$$C(E_p/\sigma_E,\alpha) = \int_{-E_p/\sigma_E}^{+\infty}\mathrm{d}y\,\varphi(y)\,\Phi(\alpha y). \tag{17}$$

While the avalanche regime distribution functions are well known in the archived literature [3], the skew normal distribution is introduced here for the first time. It contains a single local maximum in the momentum space, corresponding to a kinetic energy of the order of E_p and can be viewed as the result of stochastic processes [25], as those involved in the Fokker–Planck equation. This distribution can describe reasonably well the non-monotonic distributions with an accumulation area in the $(E,\,\theta)$ space, e.g. obtained by the solution of the RE kinetic equation (100) in [3] shown in figure 22 of that reference. A similar pattern is indeed obtained utilizing the skew normal distribution vs. the energy, as shown in figure 1. The form of the distribution function can be attributed also to the mechanism suggested for example in [26], and the EM wave emission in turn affects the distribution function, as suggested in [27].

A benchmark of the REDHPW code has been performed considering the case analyzed in section 5 of [16]. To this end, we adopt the distribution function (15) with $u_o = \sqrt{25^2-1}$ and $\sigma = 200$. This distribution is, in practice, identical to the distribution function considered in [16], proportional to the Gaussian $\exp(-\theta^2/\theta_o^2)$ with $\theta_o = 0.1$. Anomalous Doppler resonance of RE was assumed in [16] to occur for $\gamma = 25$ and $\omega_{pe}/|\Omega_e| = 0.5$.

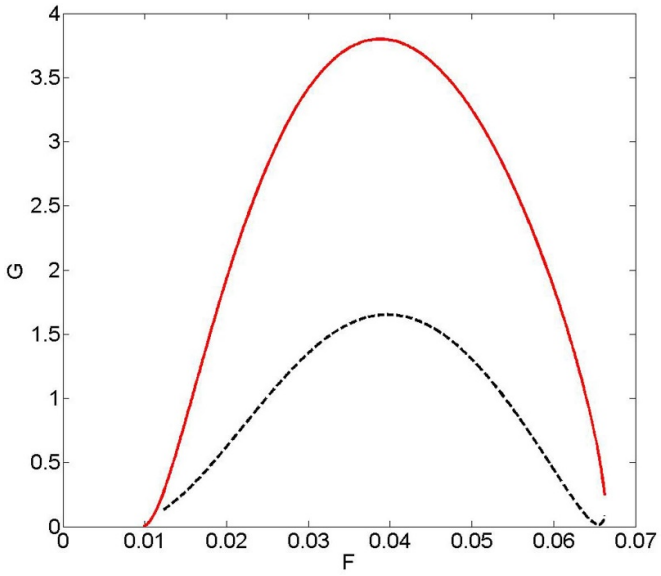

Figure 2. Normalized growth rates $G = 10^3\ \omega_i n_e/(|\Omega_{ce}|\, n_b)$ as a function of the normalized frequency values $F = \omega_r/|\Omega_{ce}|$ for the whistler waves (WW red, continuous line) and the magnetized plasma waves, i.e. lower hybrid waves (LHW, black, dashed line) considering the scenario corresponding to figure 3 of [16] (see dotted lines there for comparison). Colors online.

Here $\omega_{pe} = \left[4\pi n_e e^2/m_e\right]^{1/2}$ is the angular plasma frequency. For the benchmark, we considered pure Deuterium plasma, magnetic field with absolute value $B_o = 1.4$ T and plasma density $n_e = 4.76273\ 10^{12}\,\mathrm{cm}^{-3}$, such that $\omega_{pe}/|\Omega_e| = 0.5$. Sufficiently low temperatures ($T_e = T_i = 1.0$ eV) were considered, in order to satisfy the conditions of the cold plasma approximations for the values of the parallel and perpendicular refractive indices in the range of frequency explored. The growth rates for whistler (WW) and magnetized plasma waves (i.e. LHW), as calculated by REDHPW are shown in figure 2. The agreement with the corresponding curves shown in figure 3 (with dotted lines) of [16] is good. As a further benchmark, the approximate numerical solutions of the dispersion equation obtained by REDHPW, were compared for different plasma scenarios with the results of the code DISEMAG [28]. The latter calculates, for given parallel wavenumber and angular frequency, the relevant solution $N_\perp$ of the full dispersion equation, as given by equation (2), in the complex plane. The agreement of REDHPW and DISEMAG results is good, if performed within the limits of validity of the Taylor expansion used to find the approximate dispersion equation in REDHPW.

3. Stability analysis of re driven waves in FTU hot plasmas

RF emissions have been detected in FTU during plasma discharges with RE, both during the current ramp up phase and the flat top. The emissions were collected by ex-vessel Log-periodic antenna, designed for optimal detection in the frequency range 470–860 MHz. The antenna was located in front of a vertical port, closed for vacuum with a glass window. The port had a section of 400 mm x 160 mm, which determines a cut-off frequency close to ∼375 MHz. The signal transmission line was performed through a double-shielded 50 Ohm coaxial cable, with 10 dB/100 m attenuation at 800 MHz, about 25 m long. The acquisition system was provided by a NI PXIe-5186 digitizer, for sampling signals at a maximum rate of 12.5 GSa s^{-1} at 8 bits. The maximum frequency limit was set to ∼1.56 GHz. Though relatively low, compared to the PXI maximum capability, it allowed a good balance between resolved bandwidth and acquisition duration achievable with the on-board memory. This set ensured a maximum acquisition time window of 200 ms, sufficient, for example, to measure signals in a continuous way for most of the FTU current rump-up phase. Details of the diagnostic system are illustrated in [8]. A first account of RF emissions detected in FTU for various plasma regimes with RE is given in [6]. The measurements provided a sensitive monitor of instabilities during early RE build up phase. Broadband radio bursts as well as discrete line emissions were reported. The analysis of the time evolution of the frequency spectra of the radio bursts showed the occurrence of spectral broadening on the time scale of the amplitude e-folding time. This suggested that the rapid onset of RE instabilities after relatively long quiescent periods could be due to non-linear wave coupling. Non-linear behavior is also indicated by ringing oscillations in the time domain. The data analysis of the experiments in FTU and the comparison with the theoretical predictions allowed also to identify for the first time the presence in a tokamak discharge of lower hybrid (LH) waves driven by RE via the Cherenkov resonance [7]. A model of RE distribution vs. the parallel and perpendicular momentum, $f_{\mathrm{RE}} = n_b g(p_\parallel)\exp(-p_\perp^2/p_{\perp o}^2)/(\pi p_{\perp o}^2)$, was adopted to evaluate the growth rate of LH waves, assuming a small perpendicular spread $p_{\perp o} = 0.01$, unit slope $g'(p_\parallel = \sqrt{\gamma^2 - 1})$ at the resonance and $n_b = 10^{-3} n_e$. Here the RE momentum is normalized to $m_e c$. The cold plasma approximation was assumed. As a result, the growth rates peak at the angular frequency $\omega \cong 1.4\,\omega_{pi}$ (corresponding to an emission frequency of about 690 MHz) in good agreement with the observations. The order of magnitude of the LH growth rates was found in the range $10^{-3} - 10^{-2}\omega_{pi}$ for $\gamma = 10$, i.e. for RE energy of about 5 MeV. Here ω_{pi} is the angular ion plasma frequency. In the present study, the REDHPW code has been used to analyze FTU scenarios, with plasma and RE parameters compatible with the observations performed during the current ramp up phase and the flat top. To identify instability features associated to the presence of hot plasma background the focus is on quiescent discharges with relative high electron temperature in the RE region, of the order of 1.0 keV, and relative low RE maximum energy <22 MeV, i.e. below the threshold for synchrotron radiation in the visible range. The frequency range explored is 450–800 MHz, covering most of the FTU observations and including the range of maximum gain of the RF emissions detection antenna. Owing to the large value of the ratio $|\omega_{ce}/\gamma\omega|$ for the range of frequency considered and the relative large magnetic field of the FTU discharges, the parallel refractive index relevant for resonances in equation (1) with $n \neq 0$ is typically 10.

Table 1. Plasma and re parameters.

n_e	T_e	T_i	B_o	$Z_{\rm eff}$
1.0 10^{19} m^{-3}	2.5 keV	0.7 keV	5.3 T	3
n_b	E_P	α	σ_E	σ_o
1.0 10^{16} m^{-3}	6.0 MeV	2.0	4.0 MeV	4.0

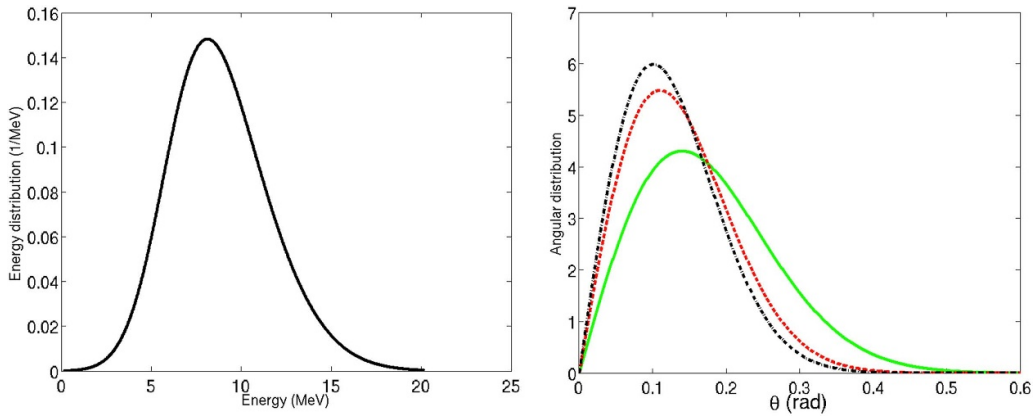

Figure 3. Energy distribution (left) and angular distributions (right) for $E = 6$ MeV (green, continuous line), $E = 10$ MeV, (red, dashed line) and $E = 12$ MeV (black, dash-dotted line with the largest peak). Colors online.

Therefore, electron Landau damping prevents the onset of kinetic instabilities.

We focus our analysis on Cherenkov resonance $n = 0$ and adopt the RE distribution function given by equation (16) to model the non-monotonic RE energy distributions envisaged in [20] for FTU. Single ion species Deuterium plasma is considered. As a first case, we consider the plasma and RE parameters reported in table 1.

The relevant energy distribution, shown in figure 3 (left), is peaked at ∼8 MeV and span 1–20 MeV energy range. The pitch angle distribution, shown in figure 3 (right), is characterized by peak angular spread in the range $\delta\theta \cong 0.1 - 0.15$ rad, i.e. typical values for RE, considering RE energies between 6 and 12 MeV. To avoid any misleading, we specify that the angular distribution in figure 3 includes the factor $\sin(\theta)$, i.e. it is a true angular distribution vs. the pitch angle, whereas the angular dependence shown in figure 1 does not include this factor, as indicated in the relevant caption. We first consider kinetic instabilities driven via Cherenkov resonance, with parallel refractive index near the value 1.0038, corresponding to the relativistic parameter $\gamma \cong 11.5$ and RE energy $E \cong$ 5.4 MeV. Near such values, the largest positive gradients of the energy distribution occur, providing a source of free energy available to drive the kinetic instabilities.

In figure 4, we show the solutions of the dispersion equation (5), as calculated by REDWPW, for the plasma parameters of table 1, $N_{\|} = 1.0038$ and considering the frequency range 450–800 MHz.

In addition to WW and LHW the solutions of the dispersion equation include two branches that cannot be identified within the cold plasma approximations, i.e. a set of EPW and IBW, which occur between two successive harmonics of

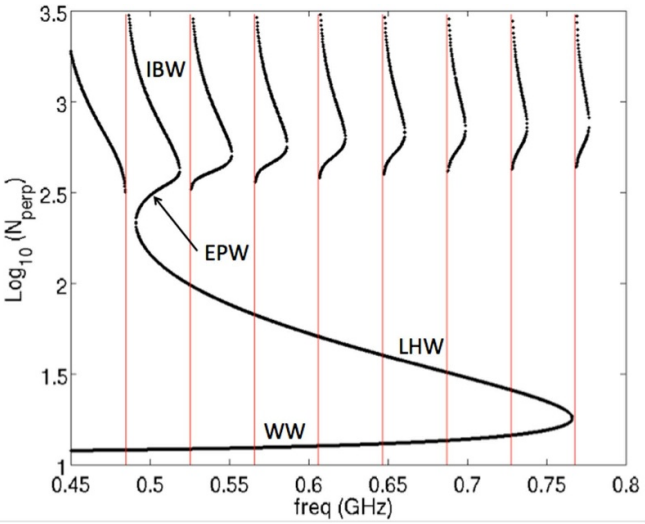

Figure 4. Solutions of the dispersion equation for $N_{\|} = 1.0038$ and plasma parameters as in table 1. The vertical red lines indicate the frequencies that are multiples nf_{ci} of the ion cyclotron frequency, from $n = 12$ (left) to $n = 19$ (right).

the ion cyclotron frequency $f_{ci} = \Omega_i/(2\pi) \cong 40.4$ MHz. We indicate only the first couple of them, occurring after the 11th cyclotron harmonics (i.e. corresponding to $n = 12, n = 1$ being the fundamental cyclotron resonance: we adopt hereinafter this nomenclature). These waves have larger perpendicular refractive index compared to WW and LHW. The EPW, with lower perpendicular refractive index than IBW, have a positive slope of $N_{\perp}$ vs. the frequency, whereas the IBW have negative slope, as the LHW, namely they are backward waves.

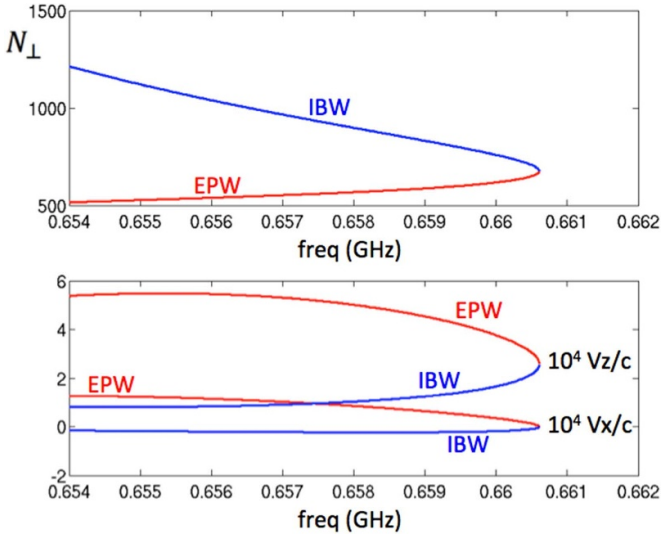

Figure 5. The perpendicular refractive index is shown vs. the frequency in the region of EPW-IBW confluence between the 15th and the 16th ion cyclotron harmonics frequency (top plot). The bottom plot shows the parallel (Vz/c) and perpendicular (Vx/c) group velocity of EPW and IBW vs. the wave frequency. Here $N_\parallel = 1.0038$. The relevant plasma parameters are listed in table 1. The EPW branch is indicated in red, the IBW branch is in blue. Colors online.

Near the confluence of these two branches, the perpendicular group velocity is crossing the zero value. This is important for the development of kinetic instabilities, since the wave packets driven unstable propagates, in this case, along magnetic field lines. Therefore, if the instabilities occur near the magnetic axis, the plasma and RE parameters are constant and significant amplification might occur. As a result of the linear stability analysis performed by REDHPW we have found that instabilities occur near all the EPW-IBW confluence points, even for frequencies larger than those in figure 4. The frequency gap between successive EPW-IBW confluences tends to increase and becomes constant approaching f_{ci} for larger frequencies. The successive frequency gaps in figure 4, after the 11th cyclotron harmonics, are about 33 MHz, 35 MHz, 36.5 MHz, 37.5 MHz, 38 MHz, 39 MHz, and 39 MHz. As an example, we consider here the instabilities driven by the RE in the frequency region near the EPW-IBW confluence between the 15th and the 16th cyclotron harmonics, at the frequency $f \cong 660$ MHz. In figure 5 we show in detail $N_\perp$ as well as the perpendicular and parallel group velocity vs. the frequency for the value of the parallel refractive index $N_\parallel = 1.0038$. Near the confluence the perpendicular group velocity crosses the zero, and the parallel velocity is $\sim 2.6\,10^{-4}c$, i.e. about $7.8\,10^6\,\mathrm{cm\,s^{-1}}$.

In figure 6, the growth rates of the EPW and IBW branches calculated by REDHPW near their confluence are plotted vs. the frequency and the parallel refractive index. As a result, the growth rates near the confluence are about $1.9\,10^5\,\mathrm{s^{-1}}$. In this scenario, owing to the low parallel refractive index, which is close to 1.0, the electron Landau damping is completely negligible. The ion cyclotron damping, which might occur in principle due to the 16th ion cyclotron resonance, is also negligible, owing to the high harmonics involved. Moreover, the collisional damping is much lower than the growth rates. The electron-ion collisional frequency in this scenario is indeed of the order of $10^4\,\mathrm{s^{-1}}$. The growth rates are thus proportional, in practice, to the concentration of the RE. As discussed above, if the wave is driven unstable by RE near the magnetic axis, the wave amplification might occur up to the saturation level. The latter is determined by the quasilinear interaction of the wave packet with the RE. The energy distribution tends to flatten in the region of wave-particle Cherenkov interaction and the positive slope is reduced up to reach the marginal stability condition. This occurs when the wave growth rate is balanced by the collisional and ion cyclotron harmonics damping.

It is possible that the electric field of the waves reach a value sufficiently high to excite LHW via nonlinear inverse Landau damping [29]. In this vein, we suggest here a picture that might explain the line emissions with frequency gap of about one half of the ion cyclotron frequency observed in FTU discharges. Three modes can be coupled by the nonlinear process, namely an IBW large amplitude wave at angular frequency ω_{IBW}, with parallel and perpendicular wave numbers $k_{\parallel,\mathrm{IBW}}$ and $\boldsymbol{k}_{\perp,\mathrm{IBW}}$, a LHW at angular frequency ω_{LHW} with wave numbers $k_{\parallel,\mathrm{LHW}}$ and $k_{\perp,\mathrm{LHW}}$ and a quasi-mode with angular frequency ω and wave numbers $k_\parallel$ and $\boldsymbol{k}_\perp$. The matching conditions required by the nonlinear interaction are

$$\omega_{\mathrm{LHW}} = \omega - \omega_{\mathrm{IBW}},\ k_{\parallel,\mathrm{LHW}} = k_\parallel - k_{\parallel,\mathrm{IBW}},\ \boldsymbol{k}_{\perp,\mathrm{LHW}} = \boldsymbol{k}_\perp - \boldsymbol{k}_{\perp,\mathrm{IBW}}. \tag{18}$$

For $\omega = (3/2)\,\omega_{\mathrm{IBW}}$ and $N_\parallel = k_\parallel c/\omega = N_{\parallel,\mathrm{IBW}}$, we obtain $\omega_{\mathrm{LHW}} = \omega_{\mathrm{IBW}}/2$ and $N_{\parallel,\mathrm{LHW}} = N_{\parallel,\mathrm{IBW}}$. This means that both the LHW at half IBW frequency and the quasi-mode are in Cherenkov resonance with the RE and supports the hypothesis that RF line emissions can be observed in this scenario with a frequency gap near the value $f_{ci}/2$.

A second scenario has been analyzed with REDWPW, corresponding to the plasma parameters listed in table 2, relevant for the observations made during the ramp up phase of the FTU shot 43 609. These parameters correspond to the major radius coordinate $R \simeq 111$ cm. We assume indeed that the RE beam is located off-axis with density peak at the magnetic surface with label R. We still adopt the RE distribution function given by equation (16) with the parameters of table 2, with the exception of the RE density, which is assumed $n_b = 2.4\,10^{16}\,\mathrm{cm^{-3}}$, i.e. 0.2% RE concentration, so that the RE current density is $\sim$1.25 MA m^{-2}. About 5 kA current can be driven by RE, if one assumes a circular cross section of the beam with 10^2 cm^2 surface area and linear shape of the current density profile vs. the radius of the section. In figure 7, analogous to the figure 4, we show the solutions of the dispersion equation (4), as calculated by REDWPW, for $N_\parallel = 1.0038$ and the frequency range 450–800 MHz.

In this second scenario, REDHPW runs confirm the occurrence of wave instabilities at the EPW-IBW confluences.

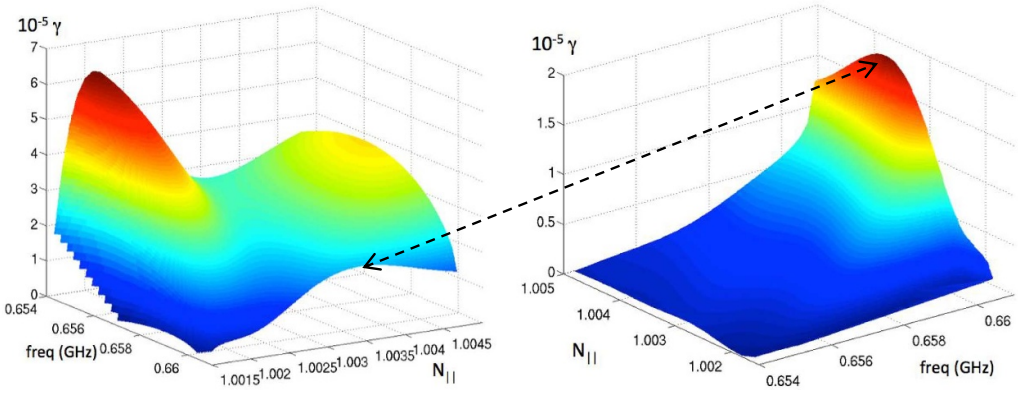

Figure 6. Growth rates γ (s^{-1}) of EPW (left) and IBW waves (right) for plasma and RE parameters of table 1. The surfaces of the two plots coalesce at the edges indicated by the double arrow in correspondence of the EPW-IBW coalescence. Note that the color scale is different in the two plots. Colors online.

Table 2. Plasma Parameters Relevant For SN 43 609.

n_e	T_e	T_i	B_o	Z_{eff}
1.2 10^{19} m^{-3}	0.6 keV	0.4 keV	4.54 T	7

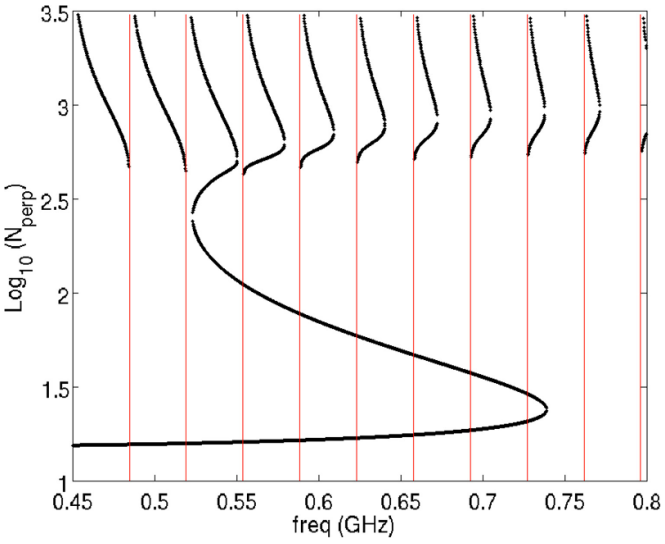

Figure 7. Solutions of the dispersion equation for $N_{||} = 1.0038$ and plasma parameters as in table 2. The vertical lines indicate the frequencies that are multiples nf_{ci} of the ion cyclotron frequency, from $n = 14$ (left) to $n = 23$ (right).

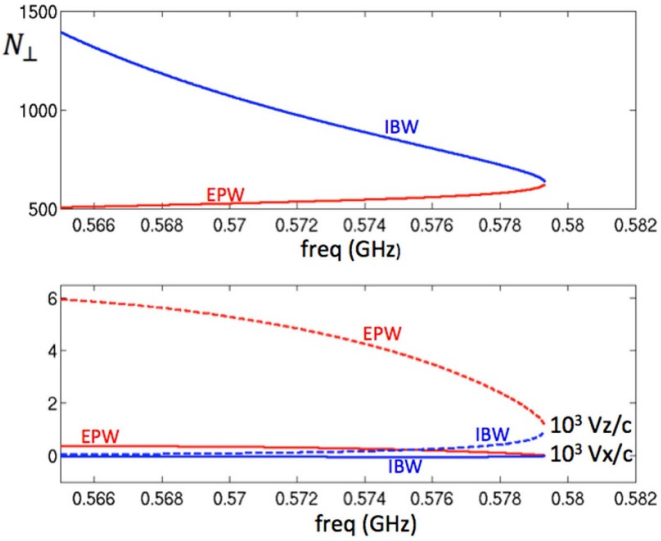

Figure 8. The perpendicular refractive index (scenario relevant for FTU SN 43 609) is shown vs. the frequency in the region of EPW-IBW confluence between the 15th and the 16th ion cyclotron harmonics frequency (top plot). The bottom plot shows the parallel (Vz/c, dashed line) and perpendicular (Vx/c, continuous line) group velocity of EPW and IBW vs. the wave frequency. The EPW branch is indicated in red, the IBW branch is in blue. Colors online.

As an example, we show the results concerning the confluence between the 15th and the 16th ion cyclotron harmonics at ∼580 MHz. In figure 8 we show in detail $N_\perp$ vs. the frequency near the confluence as well as the parallel and perpendicular velocities of the EPW and IBW branches. At the confluence the perpendicular group velocity crosses the value zero, and the parallel velocity is $\sim 10^{-3}c$, i.e. about $\sim 3.0\ 10^7\,\text{cm}\,\text{s}^{-1}$.

In figure 9, the growth rates of the EPW and IBW branches calculated by REDHPW near their confluence are plotted vs. the frequency and the parallel refractive index. As a result, the growth rates near the confluence peak at $\sim 1.1\ 10^6\ \text{s}^{-1}$. The collisional damping rates, as in the previous example, are much lower than the growth rates, though in this case the collisional frequency is larger, of the order of $10^5\ \text{s}^{-1}$, but still one order less than the growth rates. Preliminary analysis has been performed by a ray-tracing code to analyze the propagation and amplification of an IBW wave packet from an initial location at $R = 111$ cm on the equatorial plane, with 580 MHz frequency, parallel refractive index $N_{||} = 1.0038$ and perpendicular refractive index tangent to the magnetic surface. As a result, owing to the initial zero perpendicular group velocity, zero radial component of the perpendicular wave number and the fact that the IBW is characterized by parallel group velocity order of magnitude larger than the

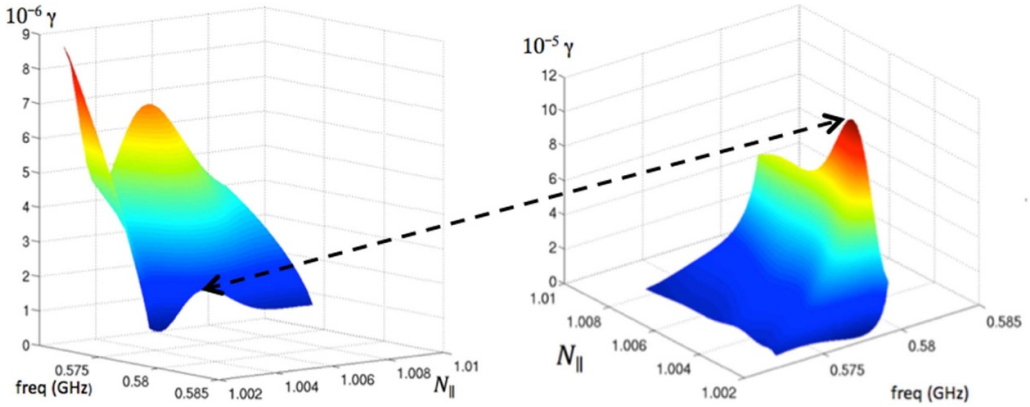

Figure 9. Growth rates γ (s^{-1}) of EPW (left) and IBW waves (right) for plasma and RE parameters respectively listed in tables 1 and 2 (but with $n_b = 2.4\ 10^{16}$ cm^{-3}). The surfaces of the two plots coalesce at the edges indicated by the double arrow in correspondence of the EPW-IBW coalescence. Note that the color scale is different in the two plots. Colors online.

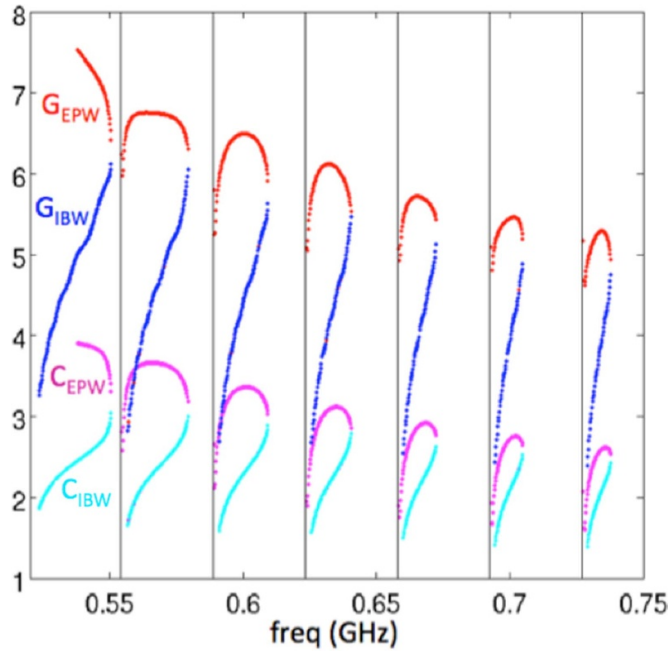

Figure 10. The growth rates and the collisional damping rates of the EPW and IBW are plotted vs. the frequency, for the plasma parameters of table 2 and the RE parameters of table 1, but with $n_b = 2.4\ 10^{16}$ m^{-3}. The red points correspond to $G_{EPW} = \log_{10}\gamma_{EPW}$, where γ_{EPW} are the growth rates of EPW in s^{-1}. The blue points correspond to $G_{IBW} = \log_{10}\gamma_{IBW}$, where γ_{IBW} are the growth rates of IBW in s^{-1}. The magenta points correspond to $C_{EPW} = \log_{10}\gamma_{EPW(C)}$, where $\gamma_{EPW(C)}$ are the collisional damping rates of EPW in s^{-1}. The cyan points correspond to $C_{IBW} = \log_{10}\gamma_{IBW(C)}$, where $\gamma_{IBW(C)}$ are the collisional damping rates of EPW in s^{-1}. The vertical lines indicate the frequencies that are multiples nf_{ci} of the ion cyclotron frequency, from $n = 16$ (left) to $n = 21$ (right). Colors online.

perpendicular group velocity, the wave packet propagate along the magnetic surface for sufficiently long time that significant amplification is expected. Depending on the initial amplitude, which should be evaluated by thermal noise or turbulent noise, wave power saturation level with sufficiently large wave amplitude might be reached to produce nonlinear effects.

Inverse Landau damping, as discussed above, can excite LHW at half frequency of the IBW. These LHW have the same parallel refractive index of the IBW and interact with RE via Cherenkov resonance.

In figure 10 we plot the growth rates and the collisional damping rates of the EPW and IBW for $N_\parallel = 1.0038$ in the frequency range 520–750 MHz.

In table 3 we list the frequencies corresponding to the EPW-IBW confluences shown in figure 7 and the relevant ion cyclotron harmonics interval where they occur. In the first column we indicate the value of the plasma density used. The frequency gaps are about $f_{ci} \cong 35$ MHz, approaching this value for larger frequencies. We list also the frequencies corresponding to the EPW-IBW confluences with the same parameters of figure 7 but lower density $1.15\ 10^{13}$ cm^{-3}.

Table 3. Frequencies (MHZ) at the EPW-IBW confluences for SN 43 609.

1.20 10^{13} cm^{-3}	550 (544.9)	579.5 (580)	609	640.5	672.5	705	738	771.5
1.15 10^{13} cm^{-3}	548.5 (557.1)	577.6	608	639.5 (645.6)	671.5 (665.4)	704.5 (702.1)	737 (740.2)	770.7

We indicate in parenthesis some frequencies that are identified in the spectrogram shown in section 3, at the time $t = 0.172$ s and at the time $t = 0.1815$ s, considering the peak of the emission line. The corresponding densities are, respectively, 1.21 10^{13} cm^{-3} and 1.15 10^{13} cm^{-3}, as given by the least squares linear regression based on the measurements performed by CO-CO_2 scanning laser interferometer, discussed in section 3.

Table 4. Observations of line emissions with $\sim f_{ci}/2$ frequency gap in FTU.

SN	time (ms)	B_o (T)	B_{res} (T)	R_{res} (cm)	$f_{ci}/2$ (MHz)
42 757	772	5.44	4.35	117	16.5
42 921	347	5.27	5.27	93.5	20
43 654	377	5.28	4.73	105	18
43 609	172	5.39	4.54	111	17.3

4. Observations of re driven hot plasma waves in FTU

Radio-frequency line emissions with frequency gap $\sim f_{ci}/2$ have been observed during various FTU discharges, as listed in table 4. There we indicate the time of the observations of the line emissions with frequency gap $\sim f_{ci}/2$, the magnetic field on axis, the magnetic field corresponding to the gap value, the corresponding major radius (the geometric center in FTU is at $R_o \sim 93.5$ cm) and the value of $f_{ci}/2$. As discussed in the previous section, the frequency gap is not exactly equal to $f_{ci}/2$ and increases with the frequency. Only a careful analysis of the experimental data by selecting the proper plasma parameters corresponding to the location of the RE beam that drives the instability can determine the set of the RF emission lines expected. Therefore, the table below is indicative of the possible locations of the RE drive of the instabilities, with the exception of SN 43 609, which has been analyzed in some detail.

The plasma current time trace of SN 43 609 is shown in figure 11(*a*); waves are observed in this case at the beginning of the flat-top phase of the discharge, during the time window indicated by the dotted vertical lines. The evolution of central density is shown in figure 11(*b*). Ion temperature and electron temperature are shown in figure 11(*c*). Plasma density profiles are measured by a two-color scanning laser interferometer. Electron temperatures profiles are measured by laser Thomson scattering. Ion temperature profiles are calculated by transport analysis performed by the JETTO code [30] using the specific version for FTU [31]. Neoclassical ion transport and constant $Z_{\rm eff} = 7$ are assumed for the JETTO analysis from $t = 0.106$ s (first available equilibrium reconstruction performed by the code ODIN [32]) to $t = 0.300$ s. The value of $Z_{\rm eff}$ used allows obtaining a reasonable agreement of the loop voltage evolution vs. time as calculated by JETTO with the measurements. The time evolution of the central ion temperature T_{io} obtained with JETTO is in good agreement with the time evolution of T_{io} calculated from neutron rate. Preliminary evaluations of the $Z_{\rm eff}$ profile, as calculated considering the bremsstrahlung emissions, confirm that the assumed average value $Z_{\rm eff} = 7$ is reasonable. Hard x-ray (HXR) emission from in-flight RE collisions with plasma ions is measured by a collimated fast electron bremsstrahlung (FEB) camera with 5 ms time resolution and 20–200 keV energy range; the FEB signal is shown in figure 11(*d*). Total HXR emission, including the one from RE impacts on plasma facing components, is monitored with 50 μs time resolution by a NE213 scintillator. The scintillator is sensitive to both HXR and neutrons; the neutron contribution to the scintillator count rate is measured by means of an array of BF3 chambers [33]. Count rates from the NE213 scintillator and from the BF3 array are shown in figure 11(*e*). The two count rates coincide in runaway-free plasmas, when signals from both diagnostics are only due to 2.45 MeV neutrons from D–D fusion reactions; the difference between the two signals is a fast and sensitive monitor for the presence of RE. The time trace of a magnetic pickup signal is shown in figure 11(*f*); some mild MHD activity is observed before the period with wave emission (170–180 ms), correlated with minor changes of the NE213 count rate.

A spectrogram of the RF emissions during the current ramp of the FTU SN 43 609 is shown in figure 12. The spectrogram shows a set of line emissions with frequency gap of about f_{ci} or $f_{ci}/2$, assuming that the emission originate at the magnetic field ~4.54 T. Seven of the line emissions predicted by the linear stability analysis can be identified within ~1.5% accuracy, as listed in table 3. A frequency drift with the time towards lower values is shown in the spectrogram. The stability analysis suggests that the frequency drift could be reproduced assuming that the density decreases with the time by ~4% from 1.20 10^{13} cm^{-3} to 1.15 10^{13} cm^{-3} in the time interval between ~172 ms and ~182 ms, which is compatible with the measured values. However, a drift of the RE towards the low field side might also explain the frequency drift, since the RE would meet lower densities and lower magnetic field values, which would decrease frequencies at the EPW-IBW coalescence. We believe this is more likely.

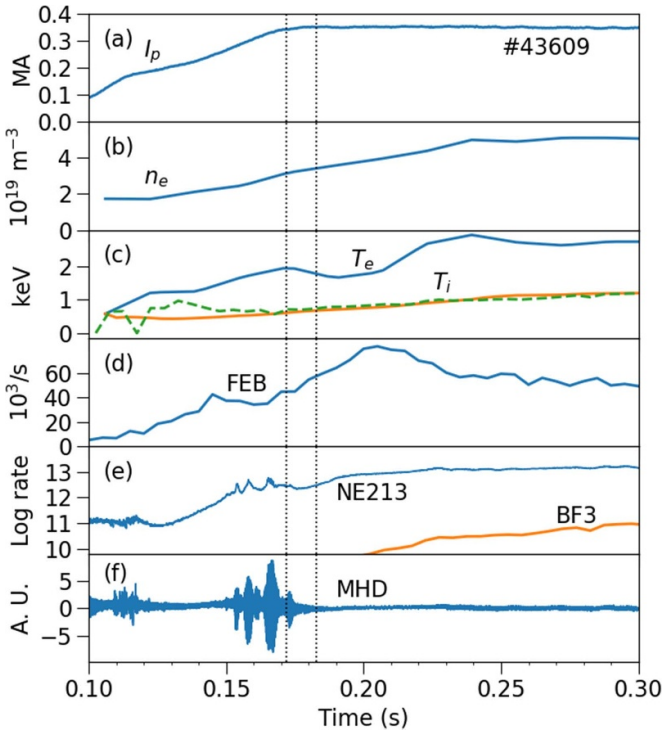

Figure 11. FTU pulse 43 609 at 5.4 T. (*a*) Plasma current in MA. (*b*) Central electron density from a CO–CO_2 scanning laser interferometer; (*c*) central electron temperature (keV) from laser Thomson scattering; central ion temperature (keV) from transport analysis (solid orange line) and from neutron rate (green dashed line). (*d*) HXR count rate from an equatorial FEB channel. (*e*) Log10 of total HXR and neutron count rate from NE213 detector, and neutron contribution from cross-calibrated BF3 detectors. (*f*) Raw magnetic pickup signal. Colors online.

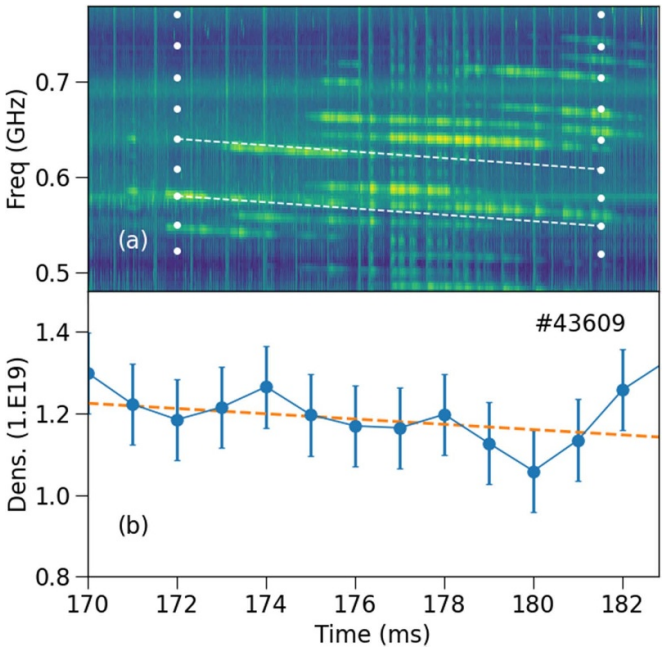

Figure 12. Spectrogram of RF emissions detected in the FTU SN 43 609 (*a*). The white circles indicate the frequencies of the modes found unstable by REDHPW at the EPW-IBW confluence, as listed in table 4. The white, dashed lines correspond to sets of line emissions predicted in the time interval from 172 ms to 181.5 ms. Time evolution of the density (*b*) as measured by CO-CO2 scanning laser interferometer at 1 ms time resolution, including the relevant error bars. The least squares linear regression line is also shown based on the interferometer data (red, dashed line). The magnetic surface considered corresponds to the major radius coordinate $R = 111$ cm on the equatorial plane. Colors online.

5. Conclusions

The stability analysis of plasma waves driven by RE has been performed considering a hot plasma background, based on the numerical code REDHPW. It calculates the dielectric tensor of non-relativistic Maxwellian magnetized plasma with multiple ion species as well the anti-Hermitian part of the susceptibility tensor of relativistic RE. In addition to standard RE distribution functions widely used, we have introduced a new kind of distribution. This is a skew-normal energy distribution [24], which seems appropriate to describe RE distributions characterized by a local maximum in the momentum space. It contains indeed a single local maximum in the momentum space and can be viewed as the result of stochastic processes [25], as those involved in the Fokker-Planck equation. Contour plots of this distribution show indeed a pattern similar to those obtained by numerical solutions of a RE kinetic equation, giving the time evolution of the distribution function of RE [3]. REDHPW provides an approximate solution of the wave equation in homogeneous magnetized plasma, based on a Taylor expansion [22]. For given Maxwellian plasma parameters and RE distribution, REDHPW identifies the normal plasma modes for a mesh of values of ω_r and $N_\parallel$. For each normal plasma mode, it calculates $N_\perp$, the electric field polarization, the wave growth or damping rate ω_i and the group velocity. In the cold plasma limit, a benchmark of the code has been performed, calculating the growth rates of WW and LHW as a function of the frequency, for specific plasma and RE parameters. A good agreement has been found with the results of the stability analysis given in [16] for a specific scenario. Stability analysis of plasma waves driven by RE in the FTU tokamak has been then performed for plasma and RE parameters reasonably compatible with the experiments aimed at the detection of radio-emission generated in the presence of RE. Quiescent discharges with Maxwellian background at ion and electron temperatures of the order of 1 keV and RE with relative small energy $<$22 MeV, below the threshold for visible synchrotron emissions are considered. The RE skew-normal energy distribution has been used, as local maximum in the energy distribution can develop in FTU since the early stages of the current ramp-up, evolving toward a quasi-monotonic behavior [20]. The solution of the dispersion equation by REDHPW in the frequency range explored, corresponding to the typical detection frequency window of the diagnostics installed in FTU, shows two additional branches with respect to those identified within the cold plasma approximation, namely the EPW and the IBW.

These waves appear between two successive ion cyclotron harmonics resonances and coalesce in correspondence of a set of frequencies with a gap almost equal to the ion cyclotron frequency f_{ci}. At the EPW-IBW coalescence, the perpendicular group velocity vanishes and the parallel group velocity is of the order of 10^7 cm s^{-1}. As a result of the analysis performed with REDHPW, growth rates of the order of 10^6 s^{-1} have been predicted to occur via Cherenkov resonance with RE for plasma waves at the EPW-IBW coalescence frequencies. Preliminary ray-tracing calculations have been performed, based on a specific code developed for IBW [28], for a IBW wave packet at a frequency of 580 MHz and parallel refractive index $N_\parallel = 1.0038$. It can be driven unstable at the coalescence with EPW on the equatorial plane of FTU at major radius $R = 111$ cm with perpendicular wave number tangent to the relevant magnetic surface. As a result, owing to the zero initial perpendicular group velocity and the fact that the IBW perpendicular group velocity is order of magnitude less than the parallel group velocity, the wave packet propagates along the magnetic surface for sufficiently long time that significant amplification occurs. The wave packet cross ion-cyclotron resonant harmonics layer with so large harmonic numbers that the relevant damping rates are much lower than the growth rates produced by the interaction with RE via the Cherenkov resonance. The electron Landau damping is negligible owing to the value of the parallel refractive index near 1. The collisional damping is also negligible, owing to the relative large electron temperature and the relative low plasma density. The IBW wave packets might be thus amplified up to a saturation level determined by the quasilinear interaction with RE. We suggest that large amplitude IBW generated at the coalescence frequencies with EPW, which are separated by a gap $\sim f_{ci}$, might excite LHW at half frequency via nonlinear inverse Landau damping. A set of line emissions with frequency gap $\sim f_{ci}/2$ are thus expected to occur in the FTU scenarios analyzed. These were indeed observed in SN 43 609 and in other FTU discharges, during the current ramp up phase and during the current flat top. The FTU SN 43 609 has been analyzed in some detail, performing a transport analysis with the code JETTO [30, 31] to evaluate the ion temperature profiles. The ion temperature is an important parameter to determine the characteristics of the EPW and IBW. The central ion temperature evolution vs. time as calculated by JETTO is in good agreement with the central ion temperature time evolution calculated from the neutron emission rates. Seven line emissions predicted to occur at EPW-IBW coalescence have been identified within $\sim$1.5% accuracy in a spectrogram of the detected radio emission. The frequencies observed drift with time towards lower values. Such drift can be reasonably well reproduced by the frequency generated at the EPW-IBW coalescence via Cherenkov interaction with RE if $\sim$4% decrease of the local plasma density occurs. A specific analysis of the density data at high resolution (1.0 ms) indicates that such density decrease with time is reliable, though the relative error of the measurements is of the order of 10%. However, we believe that the observed drift of the frequencies is more likely due to a drift of RE towards the low field side. Further work will be performed to study several line emissions due to IBW or EPW wave packets excited at the EPW-IBW coalescence by the interaction with RE. This will require an extensive analysis based on the specific ray-tracing code developed for hot plasma waves [28]. The wave power will be evaluated considering as initial condition the wave amplitude corresponding to thermal or turbulent noise. If large amplitude waves will be confirmed to occur, quasilinear calculation will be performed to evaluate the saturation level. Moreover, the excitation of LHW at half frequency of such large amplitude waves will be calculated, based on the nonlinear inverse Landau damping coefficients. Data analysis of the experiments performed in other tokamaks might be useful to

confirm the present interpretation of the line emissions detected in FTU as due to IBW hot plasma waves driven unstable at the coalescence with EPW and producing LHW at half frequency via inverse Landau damping.

Acknowledgments

The authors are grateful to Basilio Esposito and Daniele Marocco for their valuable contributions.

ORCID iDs

C. Castaldo https://orcid.org/0000-0003-2869-393X
R. Fedele https://orcid.org/0000-0003-3130-0287
W. Bin https://orcid.org/0000-0002-2050-4885
P. Buratti https://orcid.org/0000-0001-8426-3163
A. Cardinali https://orcid.org/0000-0003-4606-9903
F. Napoli https://orcid.org/0000-0002-7606-8488

References

[1] Hollmann E.M. *et al* 2015 Status of research toward the ITER disruption mitigation system *Phys. Plasmas* **22** 021802
[2] Smith H., Helander P., Eriksson L.-G., Anderson D., Lisak M. and Andersson F. 2006 Runaway electrons and the evolution of the plasma current in tokamak disruptions *Phys. Plasmas* **13** 102502
[3] Breizman B.N., Aleynikov P., Hollmann E.M. and Lehnen M. 2019 Physics of runaway electrons in tokamaks *Nucl. Fusion* **59** 083001
[4] Spong D.A. *et al* 2018 First direct observation of runaway-electron-driven whistler waves in tokamaks *Phys. Rev. Lett.* **120** 155002
[5] Heidbrink W.W., Paz-Soldan C., Spong D.A., Du X.D., Thome H.E., Austin M.E., Lvovskiy A., Moyer R.A., Pinsker R.I. and Van Zeeland M.A. 2019 Low-frequency whistler waves in quiescent runaway electron plasmas *Plasma Phys. Control. Fusion* **61** 014007
[6] Buratti P. *et al* (FTU Team) 2021 Fast dynamics of radiofrequency emission in FTU plasmas with runaway electrons *Plasma Phys. Control. Fusion* **63** 095007
[7] Bin W., Castaldo C., Napoli F., Buratti P., Cardinali A., Selce A. and Tudisco O. (FTU Team) 2022 First intra-shot observation of runaway-electron-driven instabilities at the lower hybrid frequency range under ITER-relevant plasma-wave dispersion conditions *Phys. Rev. Lett.* **129** 045002
[8] Bin W., Buratti P., Cardinali A., Castaldo C., Napoli F. and Tudisco O. (FTU Team) 2022 Measurement of electromagnetic waves from runaway electrons *Rev. Sci. Instrum.* **93** 093516
[9] Macusova E. *et al* 2021 Evolution of the runaway electron decay in response to the application of magnetic perturbations mitigation gases and active antenna *Proc. 47th EPS Conf. on Plasma Physics* (*Virtual*, *21–25 June 2021*) vol I2.106 (available at: https://info.fusion.ciemat.es/OCS/EPS2021ABS/pdf/I2.106.pdf)
[10] Casolari A. *et al* 2022 Whistler wave destabilization by a runaway electron beam in COMPASS *Proc. 48th EPS Conf. on Plasma Physics* (*Online*, *27 June–01 July 2022*) vol P2b.122 (available at: https://info.fusion.ciemat.es/OCS/eps2022pap/pdf/P2b.122.pdf)
[11] Bin W. *et al* (COMPASS Team and FTU Team) 2023 Runaway electrons instability measurement and analysis at the COMPASS and FTU devices *Proc. 5th European Conf. on Plasma Diagnostics (ECPD)* (*Rethymno, Crete, Greece*, *23–27 April 2023*) P1.7
[12] Kim M.H., Thatipamula S.G., Kim J., Choi M.J., Lee J., Lee W., Kim M., Yoon Y.D. and Yun G.S. 2020 Intense whistler-frequency emissions at the pedestal collapse in KSTAR H-mode plasmas *Nucl. Fusion* **60** 126021
[13] Breizman B.N. and Kiramov D.I. 2023 Marginal stability constraint on runaway electron distribution *Phys. Plasmas* **30** 022301
[14] Wijkamp T.A., Hoppe M., Decker J., Duval B.P., Perek A., Sheikh U., Classen I.G.J. and Jaspers R.J.E. 2024 Resonant interaction between runaway electrons and the toroidal magnetic field ripple in TCV *Nucl. Fusion* **64** 016021
[15] Wang M. *et al* 2023 arXiv:2307.06498v1
[16] Aleynikov P. and Breizman B. 2015 Stability analysis of runaway-driven waves in tokamaks *Nucl. Fusion* **55** 043014
[17] Ginzburg V.L. 1960 *Sov. Phys.—Usp.* **2** 274
[18] Nezlin M.V. 1976 Negative energy waves and the anomalous Doppler effect *Sov. Phys.—Usp.* **19** 946–54
[19] Liu C., Hirvijoki E., Fu G.-Y., Brennan D.P., Bhattacharjee A. and Paz-Soldan C. 2018 Role of kinetic instability in runaway-electron avalanches and elevated critical electric fields *Phys. Rev. Lett.* **120** 265001
[20] Esposito B., Martín-Solís J.R., Mier J.A. and Sánchez R. 2003 Dynamics of high energy runaway electrons in the frascati tokamak upgrade *Phys. Plasmas* **10** 2350–60
[21] STIX T.H. 1992 *Waves in Plasmas* (AIP) Ch 10
[22] Melrose D.B. 1980 *Plasma Astrophysics* vol 1 (Gordon and Breach Science Publishers Inc.) Ch 2
[23] Huba J.D. 2016 *NRL Plasma formulary,* NRL/PU/6790–16-614 (Naval Research Laboratory)
[24] O' Hagan A. and Leonard T. 1976 Bayes estimation subject to uncertainty about parameter constraints *Biometrika* **63** 201
[25] Andel J., Netuka I. and Zvara K. 1984 *Kibernetica* **20** 89–106 (available at: https://www.kybernetika.cz/content/1984/2/89/paper.pdf)
[26] Guo Z., Tang X.-Z. and McDevitt C.J. 2017 Models of primary runaway electron distribution in the runaway vortex regime *Phys. Plasmas* **24** 112508
[27] Guo Z., McDevitt C.J. and Tang X.-Z. 2018 Transition between resistive ballooning mode and toroidal drift wave mode at the edge of tokamak plasmas *Phys. Plasmas* **25** 032505
[28] Cardinali A., Castaldo C., Cesario R., Marco F.D. and Paoletti F. 2002 Analysis of the heating scenarios of the ion Bernstein wave (IBW) experiment in Frascati Tokamak Upgrade *Nucl. Fusion* **42** 427
[29] Porkolab M. and Chang R.P.H. 1972 Instabilities and induced scattering due to nonlinear Landau damping of longitudinal plasma waves in a magnetic field *Phys. Fluids* **15** 283
[30] Cenacchi G. and Taroni A. 1988 *JETTO: A free-boundary plasma transport code (basic version) Report* ENEA-RT-TIB–88-5
[31] Vlad G., Marinucci M., Romanelli F., Cherubini A., Erba M., Parail V.V. and Taroni A. 1998 A general empirically based microinstability transport model *Nucl. Fusion* **38** 557
[32] Alladio F. and Micozzi P. 1995 Experimental plasma equilibrium reconstruction from kinetic and magnetic measurements in the FTU tokamak *Nucl. Fusion* **35** 305
[33] Bertalot L., Esposito B., Podda S. and Rollet S. 1992 Improved calibration of the neutron yield measurement system on the FTU tokamak *Rev. Sci. Instrum.* **63** 4554